ORIGINAL ARTICLE

Effects of processing temperature and number of passes on the microstructure and mechanical properties of AA 6063 processed by cyclic expansion extrusion

V. Babu[1] · Balasivanandha Prabu Shanmugavel[1] · K. A. Padmanabhan[1]

Abstract

The effects of the working temperatures (260 °C, 200 °C and 130 °C) on microstructure formation in the AA 6063 alloy, processed upto ten passes by cyclic expansion extrusion (CEE) was studied. The microstructures of the CEE-processed specimens in the convergent and extrusion regions (center and edge) were examined after every two passes. The EBSD analysis revealed a decrease in the average grain size from 22 ± 5 μm to 2 ± 0.5 μm after four passes, with a simultaneous presence of a large fraction of HAGBs (45%) at 130 °C processing temperature. The TEM observations also confirmed the presence of nano-grains of sizes in the range of 50–100 nm. The CEE-processed specimen showed the highest improvement in hardness and ultimate tensile strength from 38 ± 3.4 HV and 118 ± 6 MPa to 122 ± 1 HV and 267 ± 2 MPa, respectively, after four passes at 130 °C. The specimens processed at 260 °C (ten passes), and 200 °C (four passes) showed moderate improvement in strength of 184 ± 3 MPa and 216 ± 3 MPa, respectively. On further straining (at 200 °C and 130 °C after six to ten passes), continuous dynamic recovery and dynamic re-crystallization took place which led to grain growth during SPD and, as a result, the alloy lost its strain hardening capacity and there was a decrease in the mechanical properties. At higher number of passes, the grains were elongated and coarsened, i.e., a non-equiaxed microstructure was seen after ten passes at 200 °C and 130 °C. In contrast, the specimen processed at 260 °C after ten passes, showed a homogeneous microstructure with near-equiaxed grains with 38% of HAGBs. A lower processing temperature produced a microstructure with a fine grain size distribution after a lower number of passes.

Keywords Cyclic expansion extrusion · AA 6063 · Microstructure · Severe plastic deformation · Grain refinement · Mechanical properties

1 Introduction

6xxx aluminum alloys are extensively used as rods/bars for structural applications on account of their good mechanical properties, in addition to their high corrosion resistance, superior weldability and lower cost compared with the 2xxx and 7xxx aluminum alloys [1, 2] 6xxx aluminum alloys are precipitation hardenable, as they contain solute elements such as Mg, Si, Fe, Ti and Cu. The precipitates can pin dislocations/grain boundaries and reduce the rate of dynamic recovery during severe plastic deformation (SPD) at relatively low temperatures [2]. The recent work of Babu et al. [2] demonstrated that the Mg_2Si precipitates suppressed the dynamic recovery in AA 6063 alloy during SPD.

Ultrafine-grained (UFG)/Nano-structured materials (NSMs) are produced using the bottom–up or top–down approaches. The bottom–up approach is used for producing specimens of limited dimensions. In the top–down approach, the coarse grains of polycrystalline solids are subjected to severe plastic deformation to enable the production of ultrafine-grain/nano-structure in bulk materials. Many researchers, Zhu et al. [3], Bay et al. [4], Hughes and Hansen [5] and Liu et al. [6], have reported difficulty in producing UFG in Al alloys through traditional routes due to their high stocking fault energy and low driving force needed for re-crystallization. Efficient grain refinement based on SPD has gained in popularity. Panigrahi et al. [7] demonstrated

✉ V. Babu
vbabume@gmail.com

1   Department of Mechanical Engineering, College
of Engineering Guindy, Anna University, Chennai 600025,
India

improvement in mechanical properties of AA 6063 using cryorolling, a SPD technique.

UFG materials are produced using several SPD techniques [8] that include equal channel angular pressing (ECAP)/equal channel angular extrusion (ECAE) [9], high pressure torsion (HPT) [10], multi-directional forging (MDF) [11], and accumulative roll-bonding (ARB) [12]. Design complexities and high tooling cost are the major challenges. Yet, these methods are used for the production of UFG microstructures due to their grain refining ability. Estrin and Vinogradov [13] reported that the age-hardenable alloys are most responsive to SPD processing and showed improvement in strength, hardness, toughness and fatigue strength. Cyclic-expansion-extrusion-based SPD techniques are of recent origin. Babu et al. [14] studied the efficiency of this process in achieving uniform grain refinement and also studied the effect of strain rate of deformation on the grain refinement in Al–Mg–Si alloy. Here, severe grain size reduction is achieved by the use of three-dimensional compressive stresses. Consequently, new extrusion-based SPD techniques, such as repetitive upsetting extrusion (RUE) [15], and twist extrusion (TE) [16] have been used for the production of bulk UFG/NS materials. Cyclic expansion extrusion (CEE), which involves simple tooling, has been shown to be one of the most efficient methods. Babu et al. [17] studied the effect of different temperature and number of passes on the mechanical properties of Al–Mg alloy and reported that lower processing temperature favors for excellent grain refinement. Cyclic multi-straining by CEE results in a homogeneous microstructure with near-equiaxed grains and improved properties. The microstructural aspects of SPD in Al alloys are well documented. Sitdikov et al. [18] reported the influence of temperature on the refinement in AA 7475 alloy. At the temperature range of 573–673 K, the UFG structure formed near grain boundaries. The formation of new grains during SPD by a transformation of low-angle boundaries (LAGBs) into high-angle boundaries (HAGBs) is a result of dynamic recovery. Thangapandian et al. [19] reported the transformation of LAGBs to HAGBs due to severe straining at room temperature processing of AA 5083 using RCS process. Working temperature is one of the most important, but least studied, experimental variables. As a result, the factors that control the development of microstructures at high temperatures have remained unidentified.

Pardis et al. [20] have presented the mechanical properties of AA 1050 after CEE. An increase in the hardness value was seen from ~ 28 HV to ~ 47 HV, along with a homogeneous microstructure after the first pass of CEE. Later, Pardis

et al. [21] investigated the effect of CEE on grain refinement in an AA 1050 alloy strip. A substantial increase in hardness from 29 HV to 53.7 HV with a fine grain structure was observed after four CEE passes. The effect of temperature on CEE was studied in none of the several studies.

In view of severe deformation of the specimen, warm working temperatures are found suitable for deformation. Working above the re-crystallization temperature leads to faster dislocation annihilation. Therefore, grain refinement may not be very effective above $0.5T_m$. In this paper, the effects on the microstructure and mechanical properties of AA 6063 alloy of three CEE processing temperatures (below the re-crystallization temperature), viz., 260 °C, 200 °C, and 130 °C ($0.4T_m$, $0.3T_m$ and $0.2T_m$, where T_m is the melting temperature of the alloy on the absolute scale) and the number of passes to which the alloy is subjected, are described.

2 Material and experimental work

The work material used was 6063 commercial aluminum alloy (AA 6063)—T6, which has a chemical composition as shown in Table 1. Cylindrical specimens with dimensions of 18-mm diameter and 130-mm length were annealed at 480 °C for 3 h in an electric furnace and then furnace cooled to room temperature.

The CEE process was employed upto 10 passes at three processing temperatures, viz., 260 °C, 200 °C, and 130 °C using a cylindrical split die extrusion setup consisting of two similar semi-die halves of angle (α) equal to 22.5° (Fig. 1). All the three processing temperatures selected were in the warm working range. The cylindrical split dies had dimensions of 100 mm diameter and length of 162 mm (i.e., 2 × split die halves with dimensions (100 mm × 81 mm). The punch and the extrusion chamber of the die had identical dimensions (diameter (D_o) ~ 18 mm). The expansion region of the die had a diameter (D_m) of 27 mm.

The schematic representations of the CEE process and the die profile are shown in Fig. 1a [17] and b, respectively. The extrusion chamber and the specimen were lubricated with MoS_2 before placing the specimen inside the die. The specimen, along with the die, was heated to the specified temperature and pressed into the CEE die cavity at a constant punch velocity of 0.2 mm s^{-1}. The CEE process was carried out on a hydraulic press of 50-ton capacity. The specimen experienced radial flow and assumed a barrel shape (step-I)—Fig. 1a. At this stage, the stopper block (base plate with plunger) was removed from the die. The die was turned

Table 1 Chemical composition of the AA 606 alloy

Elements	Si	Mg	Cu	Fe	Mn	Cr	Zn	Ti	Al
Percentage (wt%)	0.444	0.574	0.017	0.213	0.095	0.001	0.011	0.067	Balance

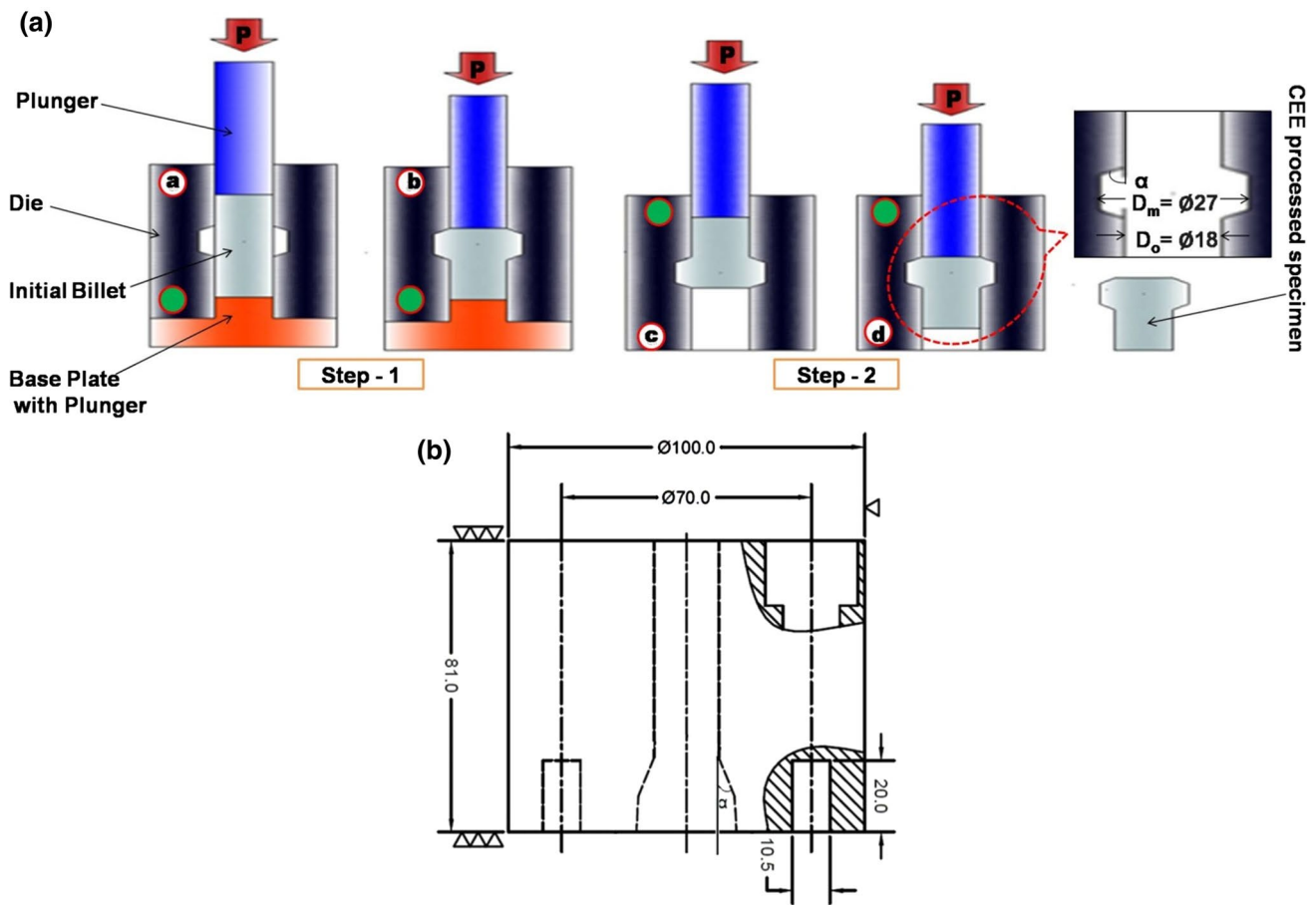**Fig. 1** **a** Experimental procedure for the CEE process, and **b** line diagram of the die profile (half of the split die) [17]

upside down (step-II) and the punch was allowed to press the specimen again allowing the material to flow into the die cavity in the opposite direction. This inward and outward flow of material together is considered as constituting a single pass. The whole cylindrical die was again turned upside down without removing the specimen. This procedure was repeated for every temperature (260 °C, 200 °C and 130 °C) upto 10 passes.

The strain (equivalent strain) induced in every pass for the present setup is given by the following equation:

$$\varepsilon = \ln\frac{D_m^2}{D_o^2} - \ln\frac{D_o^2}{D_m^2} = 4\ln\frac{D_m}{D_o}. \tag{1}$$

Using Eq. (1), the strain after the first pass was calculated as $\varepsilon \approx 1.7$, which is considerably greater than the strain induced in other SPD techniques [20].

The parent AA 6063 (annealed) and CEE-processed specimens (2–10 passes) are shown in Fig. 2a. The strain values in different regions (L1–L3) of the specimen are strongly dependent on the geometry of the die. The evaluation of the microstructure at three critical regions, namely, convergent

Fig. 2 **a** Parent AA 6063 [annealed (P)] and CEE-processed specimens (2–10 passes), **b** R1, R2, and R3 regions identified for hardness measurements, and **c** L1, L2, and L3 regions in the CEE-processed specimens considered for microstructure examination

region (L1) and extrusion regions [center (L2) and edge (L3)] of the specimen was carried out, as shown in Fig. 2b, c. TEM (JEOL JEM 2100) was used for a detailed characterization of the microstructure. Conventional polishing and wet polishing were done using 0.04 μm colloidal silica. Thin

foil specimens (along the extrusion direction) were prepared for TEM by jet polishing.

The specimens were characterized after the 2nd, 4th, 6th, 8th and 10th passes. Hardness readings were taken at regions R1, R2 and R3 in the CEE-processed specimens (Fig. 2b). A Vickers hardness (Wilson Wolpert, Germany) machine with an applied load of 500 g and a dwell time of 15 s was used for the hardness measurement. Prior to the measurement, polishing was done using SiC emery papers having 200, 400, 800, and 1200 grit sizes. The parent (annealed) and CEE-processed specimens were prepared according to ASTM E8M-89b standard [22] for the tensile testing on a 50 kN INSTRON testing machine at a constant velocity of 0.05 mm s^{-1}.

Microstructure evolution depends on the strain imparted during processing, which, to a large extent, is controlled by the semi-die angle (α) (22.5° in this case). The influence of the working temperature and the number of passes on grain refinement was analyzed using EBSD. The orientation map, grain size distribution and misorientation angles between the grain boundaries were compared among the specimens subjected to SPD by different degrees and with those present in the parent (annealed) material.

3 Results

3.1 EBSD characterization

3.1.1 Parent material

The EBSD results of the annealed AA 6063 are presented in Fig. 3 [2]. The orientation map shown in Fig. 3a consists of coarse grains of an average size of 22 ± 5 μm. Figure 3b presents the grain size distribution and variations in the grain size from 1 to 76 μm are seen. 68% of the grains were greater than 33 μm in size. Figure 3c reveals that > 87% of the grain boundaries are of the low-angle type (misorientation angle between grain boundaries < 15°).

3.1.2 CEE-processed material

The EBSD orientation maps for the CEE-processed specimens at 260 °C, 200 °C and 130 °C are shown in Figs. 4a–i, 5a–i and 6a–i, respectively. The orientation maps were taken at three critical regions of the CEE-processed specimens [i.e., convergent region (L1), extrusion region center (L2) and an edge region (L3)] in the extrusion direction (please see Fig. 2c).

After CEE processing at 260 °C, some large grains were seen in the three regions (Fig. 4a–c). The grain boundary segregation of the solutes was insignificant. Precipitation hardening and dislocation multiplication effects were limited
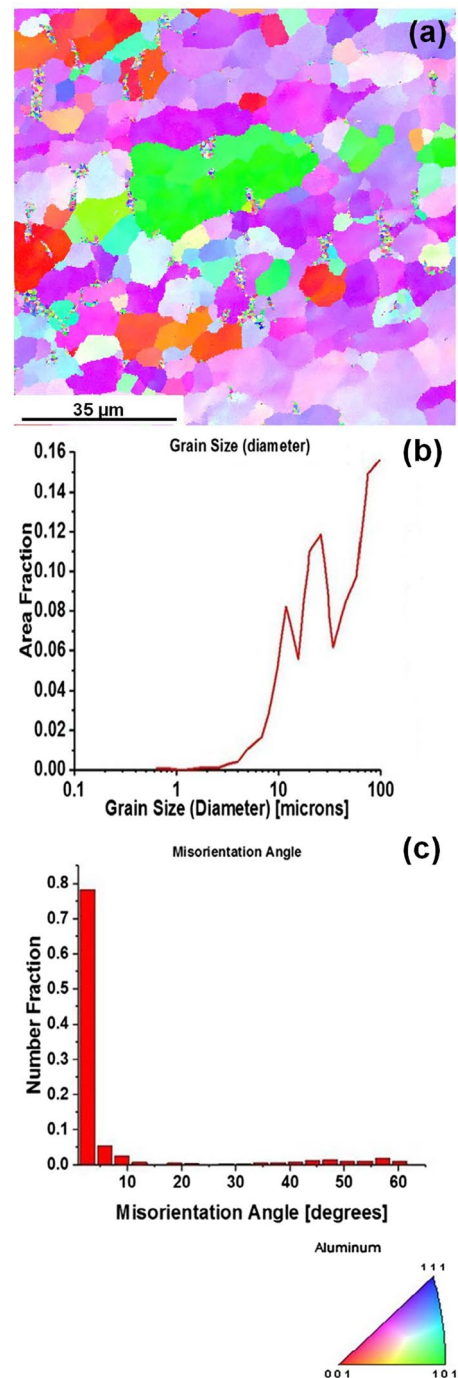
Fig. 3 EBSD pictures of parent AA 6063 material: **a** orientation map, **b** grain size distribution, and **c** histogram of misorientation angle between grain boundaries [2]

after 2 passes of CEE at 260 °C, indicative of dynamic recovery. There was evidence of grain growth and development of an inhomogeneous microstructure in the specimen processed at 260 °C. The similar observation was reported by Málek et al. [23] in Al–Zn–Mg–Cu alloy which was subjected to ECAP process at higher temperature. During
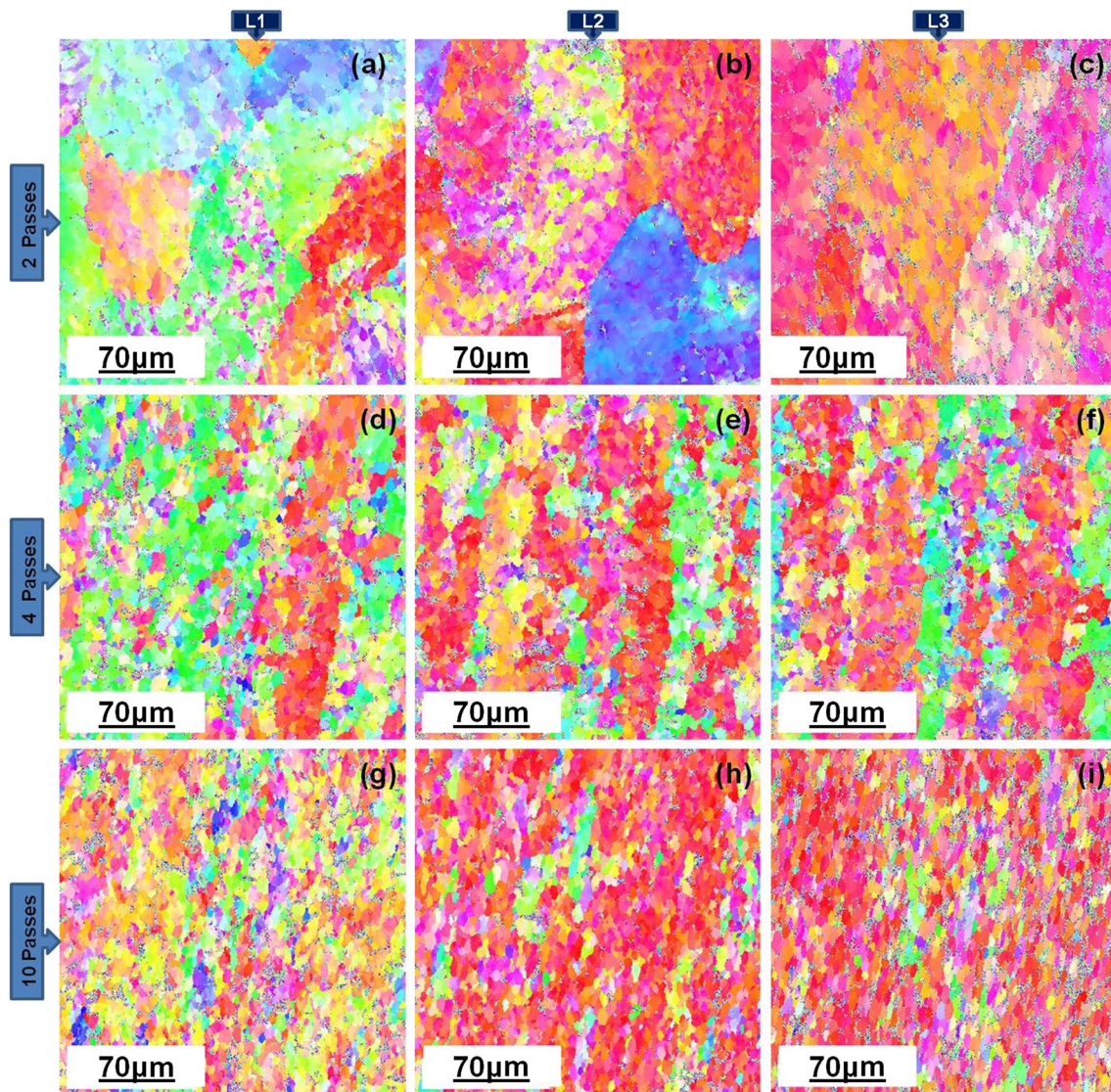
Fig. 4 EBSD orientation maps of AA 6063 alloy taken in different regions in the specimen deformed at 260 °C: **a–c** after 2 passes, **d–f** after 4 passes, and **g–i** after 10 passes in the L1, L2, and L3 regions, respectively

CEE, the material flow in every subsequent pass was in the reverse direction to that of the previous pass. As a result, the elongated grain structure got broken after 4 passes and the grain size got refined in the subsequent passes (Fig. 4d–f). The grain size was homogeneous after 10 passes at 260 °C (Fig. 4g–i).

The microstructures of the specimens processed at temperatures of 200 °C and 130 °C indicate the grains having become finer than when the processing was done at 260 °C. The fine grain size achieved by processing at these temperatures permitted shear band formation. The formation of shear bands was significant at lower processing temperatures and, based on an interaction between strain hardening, temperature softening, dynamic recovery and dynamic re-crystallization, grain refinement and subsequent grain growth

appeared. After 2 passes, the microstructure looked similar at both 200 °C and 130 °C. The formation of finer grains through a decrease in the SPD temperature is consistent with the results reported for other metals and alloys as reported by Yamashita et al. [24], Goloborodko et al. [25] and Wang et al. [26]. Yamashita et al. [24] achieved very finer grain size in pure Al and Al-3%Mg alloy at 573 K using ECAP. Goloborodko et al. [25] demonstrated the formation of UFG structure in AA 7475 alloy using ECAP after 8 passes. Wang et al. [26] also studied the effect of temperature on the microstructure of pure aluminum subjected to ECAP. At 298 K temperature, the grain refinement was significant. Figure 5a–c reveal the elongation of the grains in the extrusion direction after 2 passes at 200 °C. The microstructure had a large number of non-equiaxed grains, but there was also
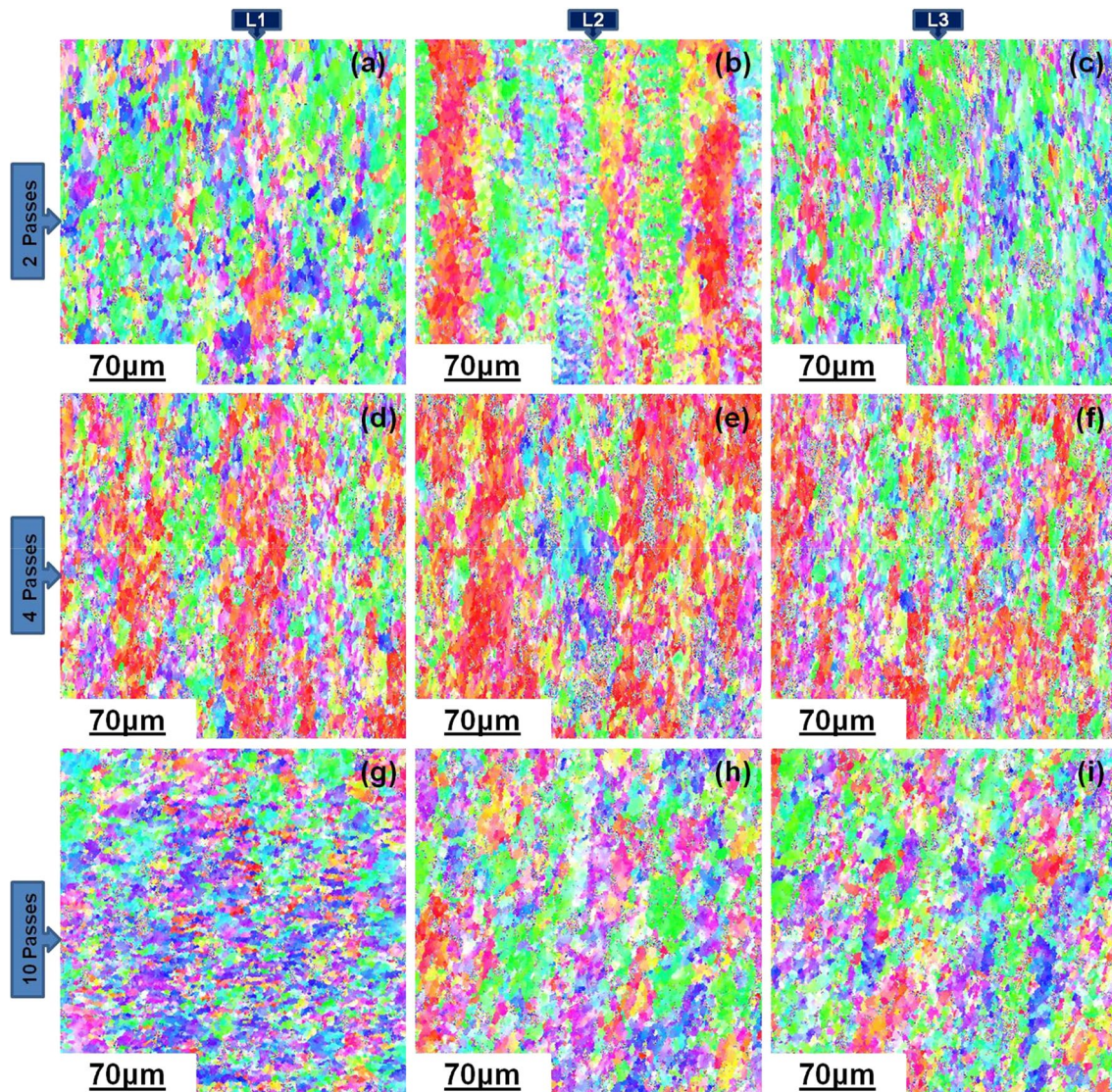
Fig. 5 EBSD orientation maps of AA 6063 alloy taken in different regions in the specimen deformed at 200 °C: **a–c** after 2 passes, **d–f** after 4 passes, and **g–i** after 10 passes in the L1, L2, and L3 regions, respectively

reasonable grain size reduction. A small fraction (2.77%) of dynamically re-crystallized grains surrounded by HAGBs was also seen—Fig. 5d–f. Multiple shearing along different directions initiated by CEE helped the formation of new sub-grains in the interior of the elongated grains, leading to the eventual spread of a new equiaxed microstructure throughout the specimen. (The new grain boundaries formed inside the coarse grains are visible in the EBSD orientation maps).

CEE processing at 130 °C led to an increase in UFG formation. In regions L1, L2, L3, the microstructure and substructure consisting of cells and sub-grains (a small fraction) were formed after 2 passes—Fig. 6a–c. Figure 6d–f shows fine grains produced after 4 passes. The orientation images reveal significant grain refinement and a homogeneous, largely equiaxed microstructure. The number of fine

grains formed at 130 °C was high after 4 passes. A majority of sub-grains, within the grains elongated in the shear direction, was equiaxed after 4 passes. The microstructure comprised a reasonable number of nano- to micron-sized grains. The microstructures of AA 6063 after 10 passes (Figs. 5g–i and 6g–i) display a slightly elongated grain size and the formation of ultrafine grains also decreased in comparison with a less number of passes (4 passes), which demonstrates the importance of dynamic recovery and dynamic re-crystallization.

3.1.3 Grain size distribution

The grain size distributions in the CEE-processed specimens at 260 °C, 200 °C and 130 °C were derived from the pole
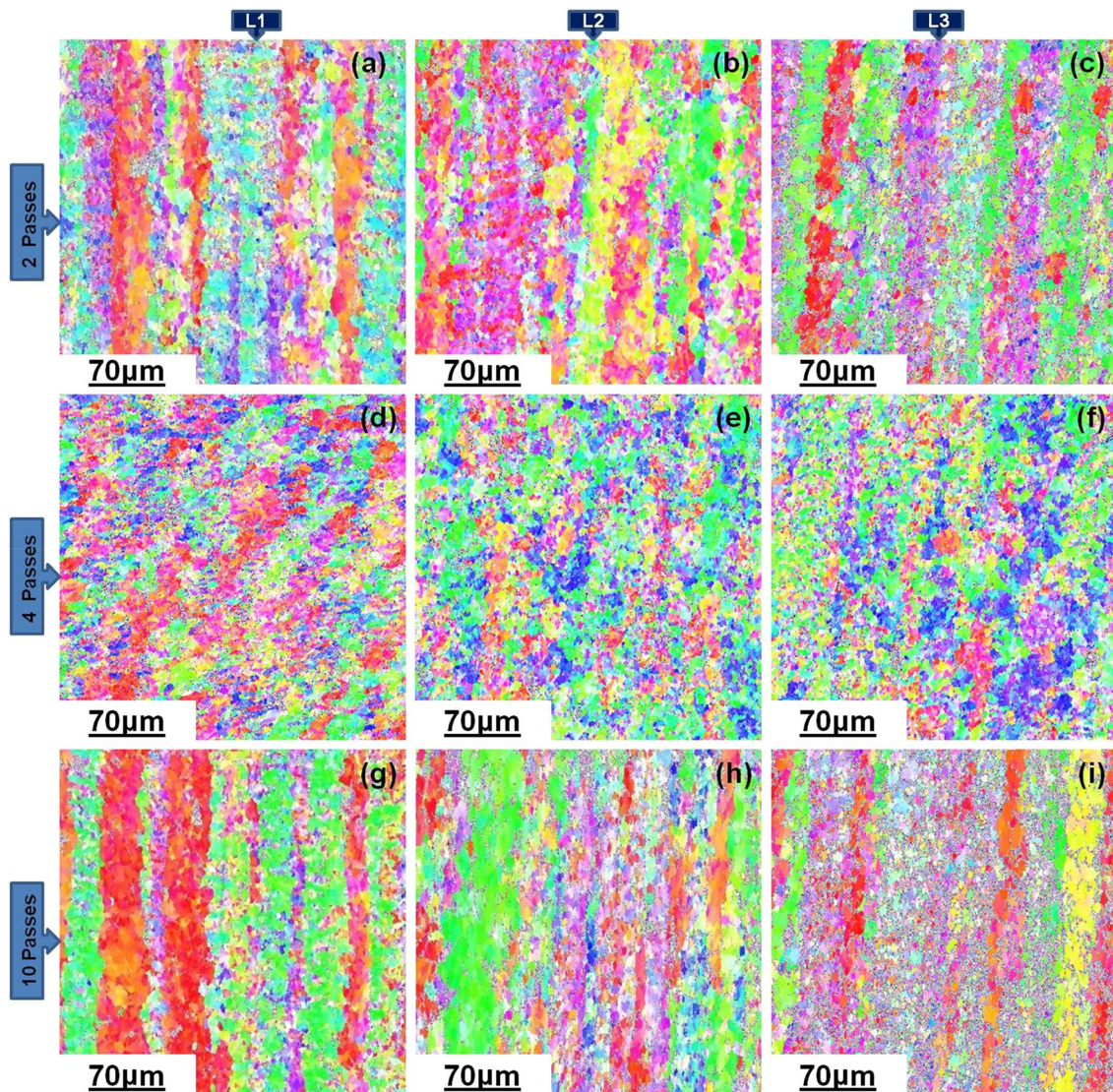
Fig. 6 EBSD orientation maps of alloy AA 6063 taken in different regions in the specimen deformed at 130 °C: **a–c** after 2 passes, **d–f** after 4 passes, and **g–i** after 10 passes in the L1, L2, and L3 regions, respectively

figures obtained from regions L1, L2 and L3. The average grain size and the fraction of grains of size less than 1 μm calculated from the grain size distributions are presented in Table 2.

Figure 4a–c, corresponding to 260 °C, displays the microstructures found after 2 passes of CEE, which consists of a small fraction of elongated and some coarsened grains. The average grain sizes in regions L1, L2 and L3 were 17 ± 3 μm, 14 ± 3 μm, and 13 ± 3 μm, respectively. The grain size details, presented in Table 2, show grain sizes smaller than 1 μm as 0.21%, 0.41% and 0.18%, respectively, in the three regions. The rest of the grains had sizes in the range of 1–10 μm. Sub-grain formation was noticed after four passes. There was a large decrease in the average grain sizes which were 8 ± 2 μm, 9 ± 2 μm, and 8 ± 2 μm in the L1,

L2, and L3 regions, respectively. The presence of ultrafine grains (< 1 μm) had increased to 0.43%, 0.70%, and 0.70% in the L1, L2, and L3 regions, respectively (Table 2). A smaller fraction (0.70%) of fine grains was observed. A reduction in the average grain size to 7 ± 2 μm (L2 and L3) after 10 passes of CEE was also noticed at this temperature (Fig. 4d–f). There was an increase in the presence of ultrafine grains (< 1 μm) after 10 passes (1.37%)—Fig. 4g–i. With an increase in the number of passes, the grain sizes in the different regions of the specimen became more homogeneous due to the stabilization of structure.

The grain size data of the CEE-processed specimens at 200 °C after 2 passes revealed the average grain sizes as 6 ± 2 μm, 7 ± 3 μm, and 6 ± 2 μm in the L1, L2, and L3 regions, respectively, Fig. 5a–c. Grains with sizes less than

Table 2 The average grain size and fraction of fine grains at different regions in the CEE-processed specimens as a function of the number of passes and processing temperatures

T (°C)	2 passes						4 passes						10 passes					
	L1		L2		L3		L1		L2		L3		L1		L2		L3	
	AVG	< 1 µm	AVG	< 1 µm	AVG	< 1 µm	AVG	< 1 µm	AVG	< 1 µm	AVG	< 1 µm	AVG	< 1 µm	AVG	< 1 µm	AVG	< 1 µm
260	17	0.214	14	0.407	13	0.179	8	0.433	9	0.703	8	0.704	14	1.486	7	1.371	7	1.229
200	6	0.908	7	1.176	6	1.242	6	1.572	5	2.775	5	2.823	8	1.925	12	1.815	8	1.665
130	7	0.845	7	1.451	6	1.174	2	5.213	2	7.257	2	7.741	5	0.837	8	0.672	5	0.601

T processing temperature, *AVG* average grain size in µm, and 1 µm < percentage of grains less than one micron

1 µm had increased to 0.91%, 1.18% and 1.24% in the L1, L2, and L3 regions, respectively. Figure 5d–f display the microstructures found after 4 passes of CEE, which consisted of a small fraction (1.57%) of elongated grains aligned in the extrusion direction. After 4 passes, a reduction in the average grain sizes to about 6 ± 3 µm, 5 ± 2 µm, and 5 ± 2 µm in the L1, L2, and L3 regions, respectively, was seen. The ultrafine grains occupied about 1.57%, 2.77% and 2.82% in the L1, L2, and L3 regions, respectively. The grains were slightly coarsened, and increases in the average grain sizes to 8 ± 3 µm, 12 ± 4 µm, and 8 ± 3 µm in the L1, L2 and L3 regions, respectively, were seen after 10 passes (Fig. 5g–i).

The specimen processed at 130 °C showed reasonable evidence of UFG formation. The grains were highly refined and the average grain sizes were reduced to 7 ± 3 µm, 7 ± 3 µm, and 6 ± 2 µm in the L1, L2 and L3 regions, respectively, after 2 passes (Fig. 6a–c). A grain size < 1 µm covered an area of about 0.84%, 1.45% and 1.17% in the L1, L2 and L3 regions, respectively, after 2 passes at 130 °C. Further, with an increase in the number of passes, fine grain formation had become very high after 4 CEE passes (Fig. 6d–f). The average grain size was reduced to 2 ± 0.5 µm after 4 passes of CEE in all the three regions. Ultrafine grains after 4 passes of CEE constitute about 5.21%, 6.25%, and 7.74% in the L1, L2 and L3 regions, respectively, see also Table 2. However, the grain size distribution after 10 passes shifted toward larger grain sizes and these values were 5 ± 3 µm, 8 ± 3 µm and 5 ± 2 µm in the L1, L2 and L3 regions, respectively (Fig. 6g–i).

3.1.4 Grain boundary misorientations

The grain boundary misorientation details of the CEE specimens processed at 260 °C, 200 °C and 130 °C are presented in Figs. 7, 8, and 9, respectively. Grain boundary misorientation angle fractions obtained from the EBSD data for the specimens subjected to 2, 4, and 10 passes at 260 °C are shown in Fig. 7a–i. The high-angle grain boundary (HAGB) fractions after 2 passes were around 17%, 16%, and 8% in the L1, L2, and L3 regions, respectively, as shown in Fig. 7a–c. With increasing strain, after 4 passes, the high-angle grain boundary (HAGB) fractions had increased to 48%, 43% and 40% in the L1, L2, and L3 regions, respectively (see Fig. 7d–f). After 10 passes, slight decreases in the HAGB fractions were seen (Fig. 7g–i), which are about 33%, 49% and 38% in the L1, L2, and L3 regions, respectively.

Boundary misorientation angles for the specimens subjected to 2, 4, and 10 passes at 200 °C are presented in Fig. 8a–i. The specimens after 2 passes, contained HAGB fractions of about 47%, 30%, and 44% in the L1, L2, and L3 regions, respectively, Fig. 8a–c. After 4 passes, the HAGB fractions were about 44%, 35%, and 40% in the L1, L2, and L3 regions, respectively, as seen in Fig. 8d–f. After 10
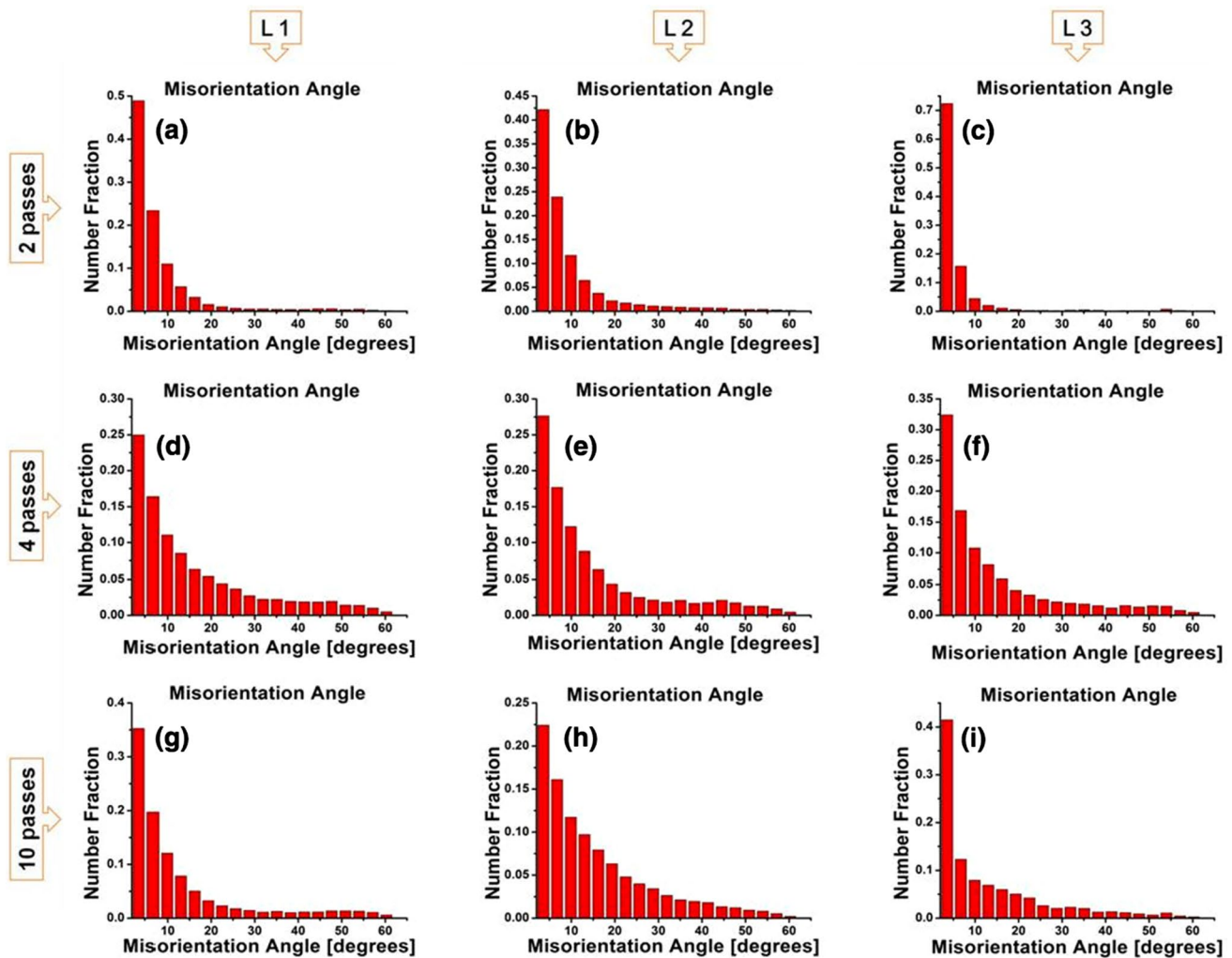
Fig. 7 EBSD misorientation angle fractions of boundaries in AA 6063 alloy CEE processed at 260 °C: **a–c** after 2 passes, **d–f** after 4 passes, and **g–i** after 10 passes in the L1, L2, and L3 regions, respectively

passes, increases in the HAGB fractions were observed as 48%, 37%, and 40% in the L1, L2, and L3 regions, respectively, see Fig. 8g–i.

Figure 9a–i presents the boundary misorientations angle fractions in the specimens processed at 130 °C. After 2 passes, the HAGB fractions were about 17%, 18% and 20% in the L1, L2, and L3 regions, respectively, Fig. 9a–c. The specimens after 4 passes had HAGB fractions of ∼ 36%, 44% and 45% in the L1, L2, and L3 regions, respectively, as shown in Fig. 9d–f. However, after 10 passes, the HAGB fractions seen of ∼ 23%, 12% and 9% in the L1, L2, and L3 regions, respectively, were once again smaller (Fig. 9g–i).

3.1.5 TEM characterization

Transmission electron micrographs (TEM) of the parent (annealed) and CEE-processed specimens subjected to 2, 4 and 10 CEE passes at 260 °C, 200 °C, and 130 °C are presented in Figs. 10 and 11a–i, respectively. The TEM images were taken at the extrusion [center (L2)] region of the CEE-processed specimens in the direction of extrusion (see Fig. 2c). Figure 10 displays a TEM image of the parent AA 6063, which consists mainly of coarse grains and very few dislocations. Figure 11a–c, d–f and g–i corresponds to the TEM images of AA 6063 CEE-processed at 260 °C, 200 °C, and 130 °C by 2, 4 and 10 passes, respectively. The severely strained sub-grains (Fig. 11a–i) under different conditions (i.e., different temperatures and number of passes) are evident from these figures. Some undeformed large grains were also seen. Figure 11a reveals the presence of elongated coarse grains (enclosed by big arrows) with a few dislocations after 2 passes. A heavily deformed microstructure was observed in the 260 °C specimen with non-uniform grain sizes—Fig. 11b. The TEM image of the CEE-processed specimen shows evidence of the presence of UFG structure (Fig. 11c).
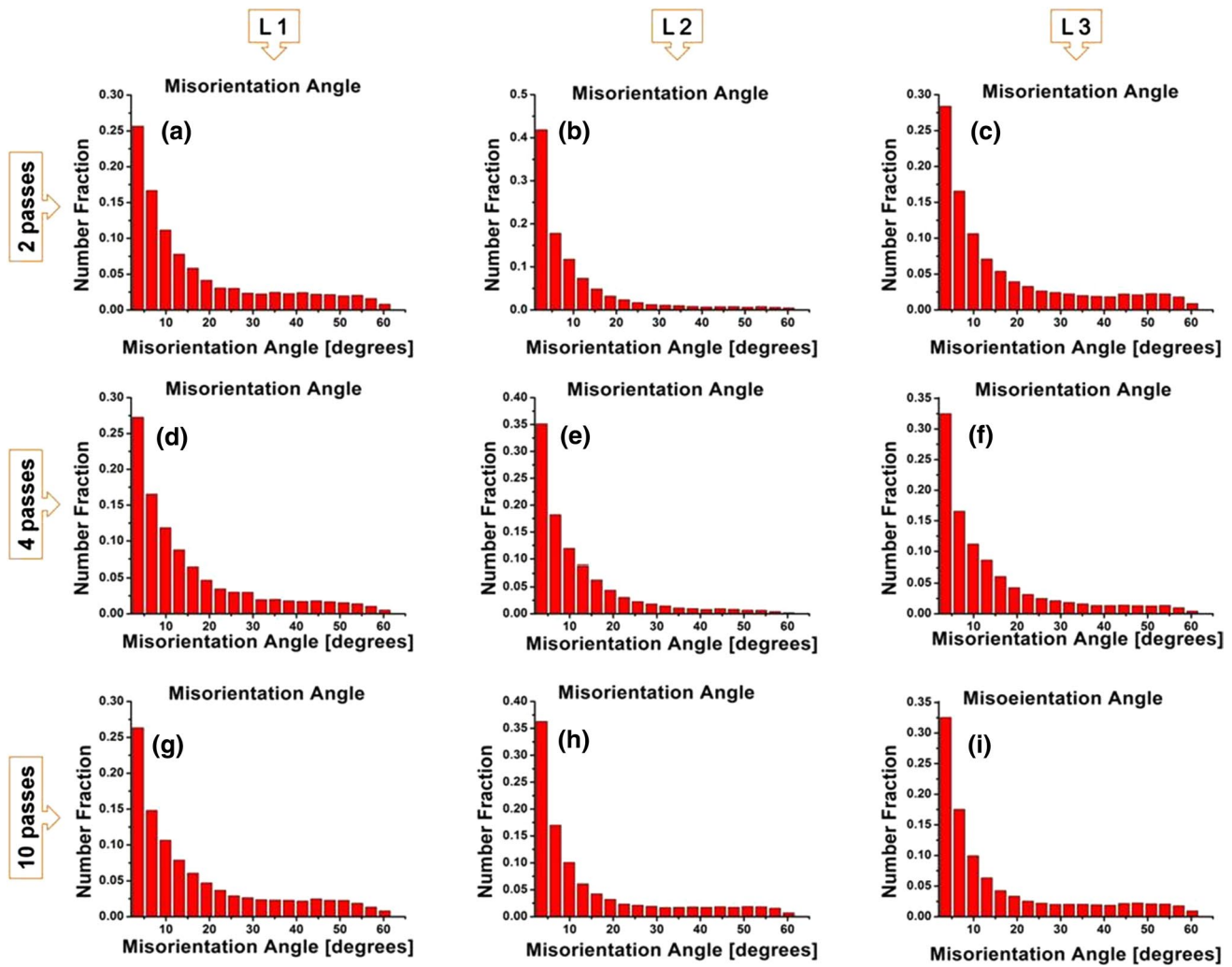
Fig. 8 EBSD boundary misorientation angle fractions in the AA 6063 alloy CEE processed at 200 °C: **a–c** after 2 passes, **d–f** after 4 passes, and **g–i** after 10 passes in the L1, L2, and L3 regions, respectively

CEE-processed specimens at 200 °C and 130 °C after 2 passes displayed dislocation cells, dense dislocation walls and dislocation tangled zones (Fig. 11d, g), respectively. However, a much lower dislocation density with ill-defined sub-grains was observed in the 260 °C alloy specimen. The TEM examination revealed the presence of elongated grains (enclosed inside arrows), large dislocation rings and elongated sub-grains (Fig. 11g). Dislocation tangles as observed at 200 °C and 130 °C alloy specimens were rarely seen in the 260 °C specimen (Fig. 11e, h). The activation of different slip systems converted grains into sub-grains, which led to a homogeneous structure at 200 °C after 4 passes—Fig. 11e. In the 130 °C specimen after 4 passes, equiaxed sub-grains with well-defined boundaries were observed. Figure 11h presents a microstructure characterized by small dislocation cell blocks formed after 4 CEE passes by many intersecting elongated boundaries along different directions as a result

of the activation of different slip systems. Notwithstanding the above, a deformed microstructure with some elongated sub-grains was observed in the 200 °C and 130 °C specimens (Fig. 11f, i).

3.2 Tensile strength

Figures 12, 13, and 14 display the stress–strain curves for specimens processed at 260 °C, 200 °C and 130 °C and subjected to different number of passes (parent and 2–10 passes), respectively. The ultimate tensile strength (UTS) at 260 °C increased from 118 ± 6 MPa to 162 ± 3 MPa, 170 ± 4 MPa, 176 ± 3 MPa, 180 ± 2 Mpa, and 184 ± 2 MPa after 2, 4, 6, 8 and 10 passes of CEE which were 37%, 44%, 49%, 53% and 56% more, respectively, compared with the parent (annealed) material—see Fig. 12.
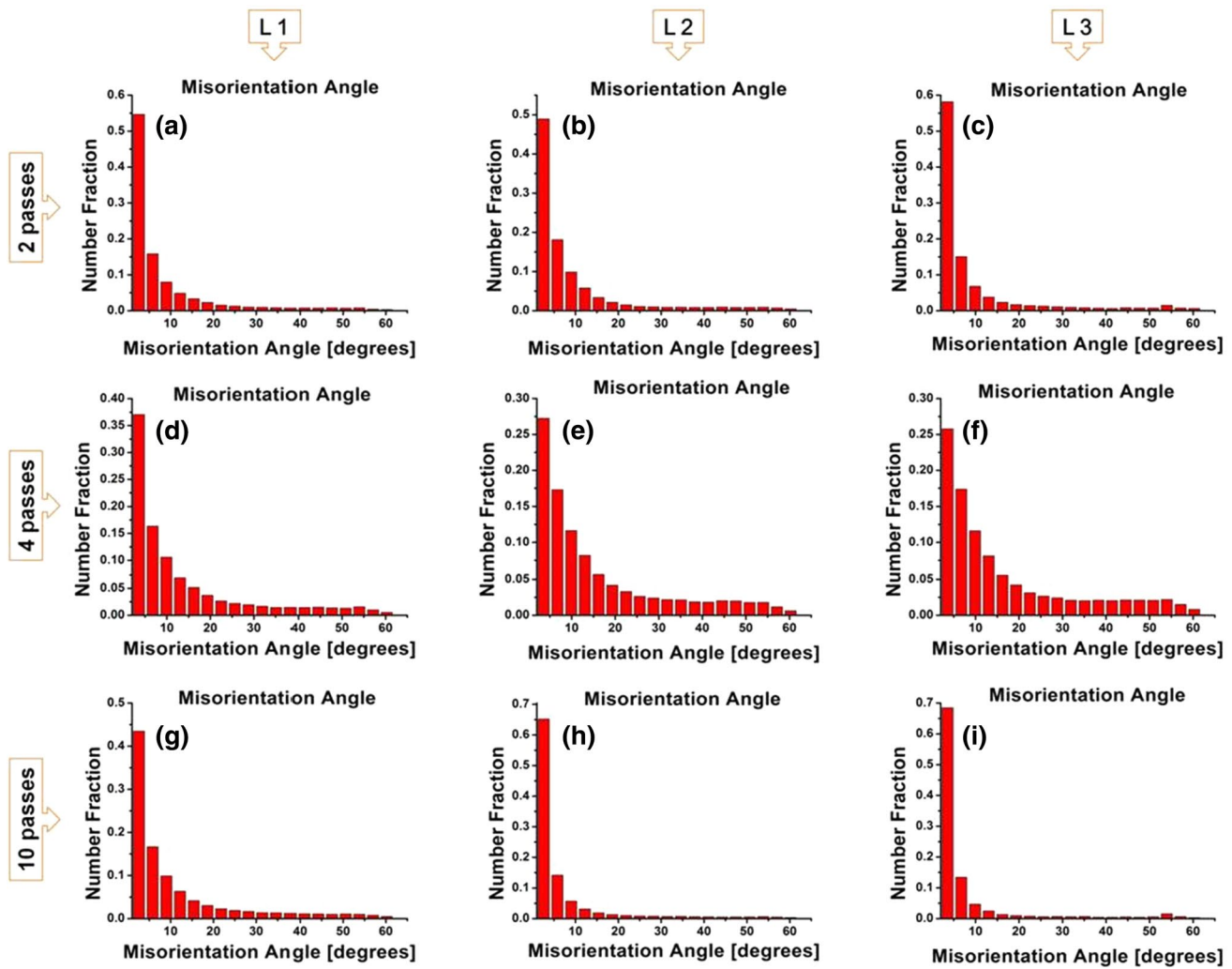
Fig. 9 EBSD boundary misorientation angle fractions in the AA 6063 alloy CEE processed at 130 °C: **a–c** after 2 passes, **d–f** after 4 passes, and **g–i** after 10 passes in the L1, L2, and L3 regions, respectively

Figures 13 and 14 show that a maximum UTS of 216 ± 2 Mpa, and 267 ± 2 MPa is seen after 4 passes at 200 °C and 130 °C, respectively. Significant increases in the UTS values were seen after 2 and 4 passes at 200 °C and 130 °C. However, there was a slight decrease [(185 ± 3 MPa, 189 ± 2 MPa, and 195 ± 2 MPa at 200 °C) and (212 ± 2 MPa, 219 ± 2 MPa, and 229 ± 2 MPa at 130 °C)] in the UTS values after 6, 8, and 10 passes of CEE at these temperatures, which, however, were higher than what is seen in the parent material. The AA 6063 specimens CEE processed at 130 °C exhibited the lowest ductility (14%) compared with an 18% elongation seen after 4 passes at 200 °C. The specimen processed at 260 °C showed good ductility (22%) after 10 passes and the ductility was about 23% in the parent (annealed) material.

3.3 Hardness

Details of hardness measurement in three different regions R1, R2 and R3 at regular intervals of 1 mm on the CEE-processed specimens are shown in Fig. 2b. The values corresponding to different processing conditions are presented in Fig. 15a–c. Increase in hardness with every pass is seen Fig. 15a. Significant variations in hardness values were seen. These were caused by differences in grain size and strain. However, the hardness of the CEE-processed specimens was always greater than that of the parent material. The scatter in the results decreased with increasing strain due to deformation becoming more homogeneous with an increase in the test temperature. Grain size variation was minimal after 10 passes and the hardness value was nearly constant. The variations in hardness values closely
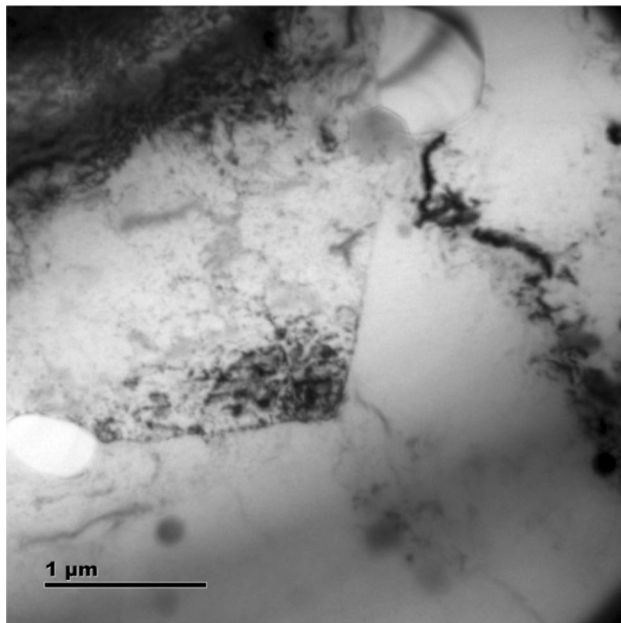
Fig. 10 TEM image of parent AA 6063 (annealed) material [2]

parallel the variations in the strength properties (YS and UTS) and the reasons for the same are similar (hardness and yield stress are directly related; in fact (hardness/3) ≈ yield stress [14].

The parent (annealed) AA 6063 showed an average hardness value of 38 ± 3.4 HV. At 260 °C, the hardness value marginally increased (75 ± 1.9 HV, 83 ± 2.9 HV, 88 ± 3.9 HV and 90 ± 3.6 HV after 2, 4, 6 and 8 passes, respectively) all the way upto ending at 95 ± 1 HV after 10 passes. There was only marginal improvement after every pass. The graph showing the deviation in the hardness values in the specimens after 10 passes at 260 °C proves that the strain imposed during higher temperature processing is more homogeneous at higher number of passes (Fig. 15a).

The specimens processed at 200 °C, in contrast, displayed a considerable increase in hardness 105 ± 1.4 HV up to 4 passes. Slight decrease in hardness at this processing temperature after every pass (6–10 passes) was seen. After 6–10 passes (95 ± 2.6 HV, 96 ± 1.5 HV and 98 ± 1.1 HV, respectively), there was no significant difference in the hardness between the processed alloy specimens at this temperature (Fig. 15b). Similarly, there was a considerable increase in hardness of 122 ± 1 HV upto 4 passes at 130 °C. After every pass (6–10 passes), there was a slight decrease in hardness at this processing temperature. After 6–10 passes (104 ± 1.5 HV, 106 ± 2 HV and 108 ± 1.5 HV, respectively), there was no significant difference in the hardness values at this temperature (Fig. 15c). However, the increase in hardness was significant after higher number of passes compared with the parent alloy.

4 Discussion

Many reports, Babu et al., Das et al., and Rao et al. [2, 10, 11] have examined the relationship between the mechanical properties and microstructures in materials subjected to SPD. The final grain size is achieved by a dynamic balance between grain refinement and grain growth. Experimental results suggest that lower recovery rates in the CEE-processed alloys facilitate the development of homogeneous microstructures. The microstructure of the annealed (Parent) AA 6063 was equiaxed, but had only a small percentage (13%) of HAGBs (see Fig. 3c). The CEE-processed AA 6063 showed significant differences in the microstructure after each pass. A comparison between the microstructures seen at 260 °C, 200 °C, and 130 °C leads to the conclusion that the grain size becomes coarser with an increase in the temperature of CEE processing. After 2 passes (a low strain), higher fractions of low-angle grain boundaries (LAGBs) were observed at all three temperatures—Figs. 7a–c, 8a–c, and 9a–c. With an increase in strain (beyond 4 passes), a marked decrease in the LAGBs and a corresponding increase in the high-angle grain boundaries (HAGBs) were observed in all three cases—Figs. 7d–f, 8d–f, and 9d–f. The fraction of LAGBs observed was higher in the 130 °C specimen at low strains (2 passes) compared with those corresponding to the 200 °C and 130 °C specimens. But, in the range of 4–10 passes, the proportion of HAGBs had increased in all three cases—Figs. 7d–i, 8d–i, and 9d–i. The migration of solutes to GBs upto 4 passes increased with the number of passes (Fig. 11d–i).

The TEM images revealed the presence of precipitates at the grain boundaries—Fig. 11a–c. The dislocations formed a ring-like structure inside the elongated grains (enclosed by arrows)—Fig. 11b. Shear bands of width of 500–800 nm in the cross-section and elongated grains were also seen at 260 °C (Fig. 11c). The precipitates pin the GBs and restrict grain growth. With an increase in the number of passes, a significant grain refinement led to improvements in the tensile strength and hardness values (Hall–Petch effect)—Figs. 12 and 15a. The microstructure displayed a lamellar boundary (arrowed), ring-like dislocation networks and elongated sub-grains (Fig. 11d). After 4 passes, the formation of equiaxed fine grains was also seen. UFGs in the range of 200–400 nm sizes could also be observed after 4 passes at 200 °C (enclosed inside arrows in Fig. 11e). A relatively homogeneous structure with HAGBs was obtained after 4 passes. Nano-grains in the range of 50–100 nm size were also observed (arrowed) after 4 passes at 130 °C—Fig. 11h. The second phase (precipitate) particles developed into points of stress concentration, facilitating dislocation generation. They also act as
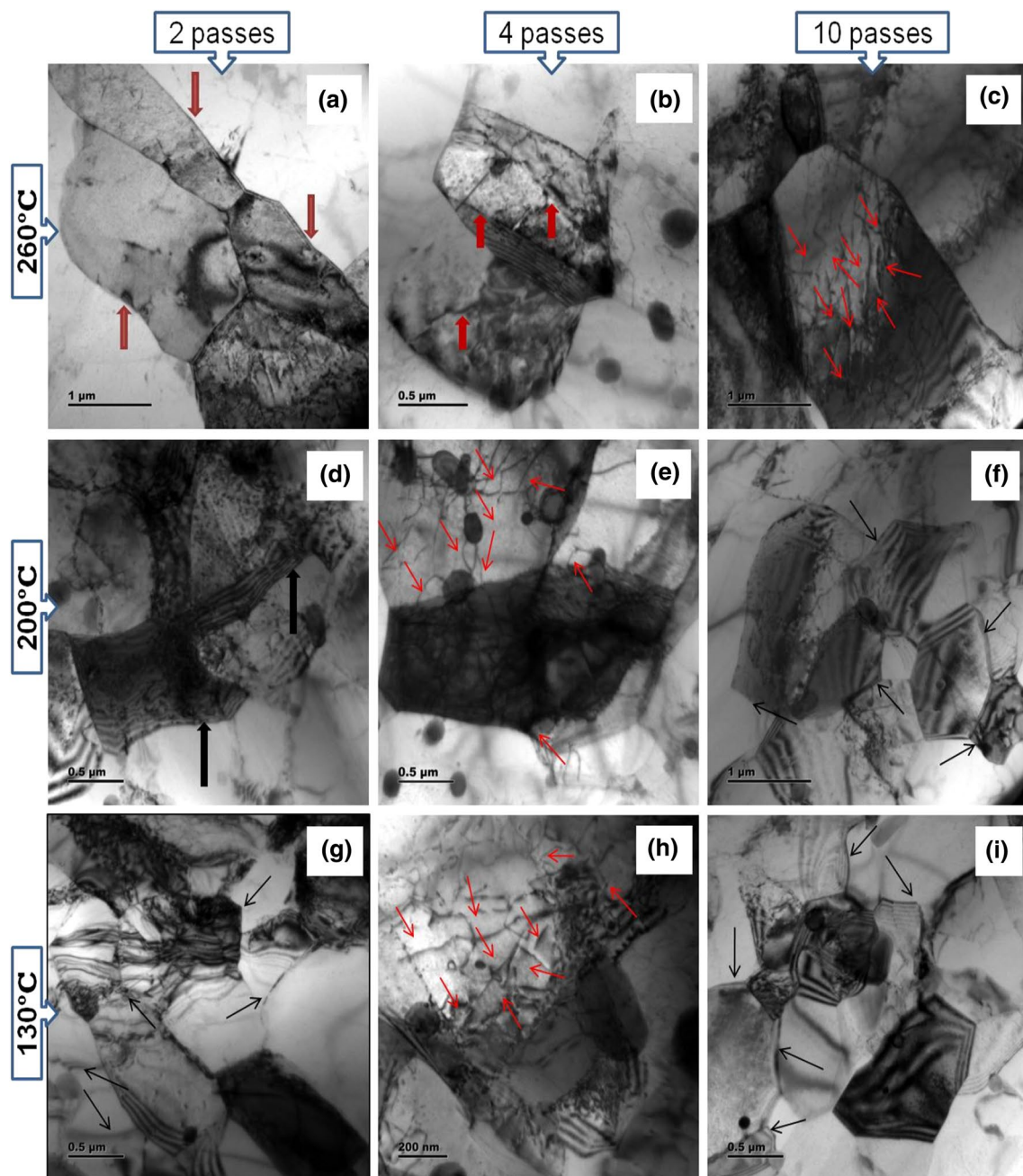
Fig. 11 TEM pictures of AA 6063 alloy specimens CEE processed **a–c** after 2, 4 and 10 passes at 260 °C; **d–f** after 2, 4 and 10 passes, respectively, at 200 °C; **g–i** after 2, 4 and 10 passes, respectively, at 130 °C

obstacles to dislocation motion, seen in the form of tangles around these precipitates as reported by Thangapandian et al. [19]. A further increase in the number of CEE passes (6–10 passes) at 200 °C and 130 °C caused a decrease in fine grain formation—again, a result of dynamic recovery. The above considerations ensured maximum grain refinement after 4 passes during processing at 130 °C—Fig. 6e, f. As a result, there was an increase in the tensile strength by about 56, 83, and 126% (184 ± 3, 216 ± 3,

and 267 ± 2 MPa) for specimens processed at 260 °C (10 passes), 200 °C (4 passes) and 130 °C (4 passes), respectively. The UTS of the parent (annealed) specimen was 118 ± 6 MPa. This is consistent with the known fact of dynamic recovery and dynamic re-crystallization becoming more dominant with increasing temperature. Further straining (6–10 passes) led to grain growth during SPD and, as a result, the alloy lost its strain hardening capacity. This led to a decrease in hardness and the ultimate
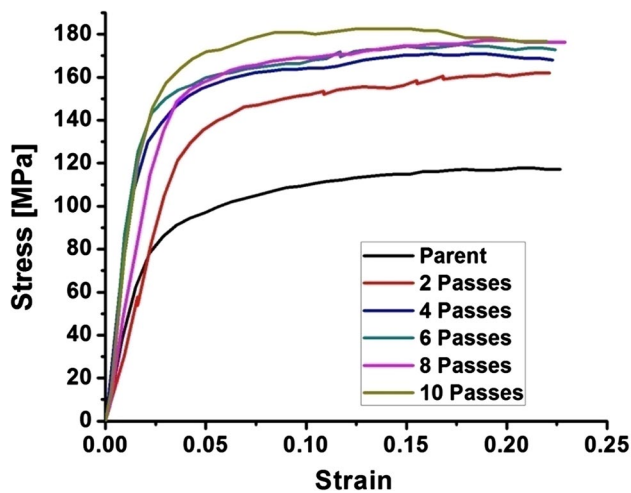
Fig. 12 Stress vs. strain curves for the AA 6063 alloy processed at 260 °C. Data concerning the parent (annealed) as well as CEE-processed AA 6063 alloy after 2, 4, 6, 8 and 10 passes are presented
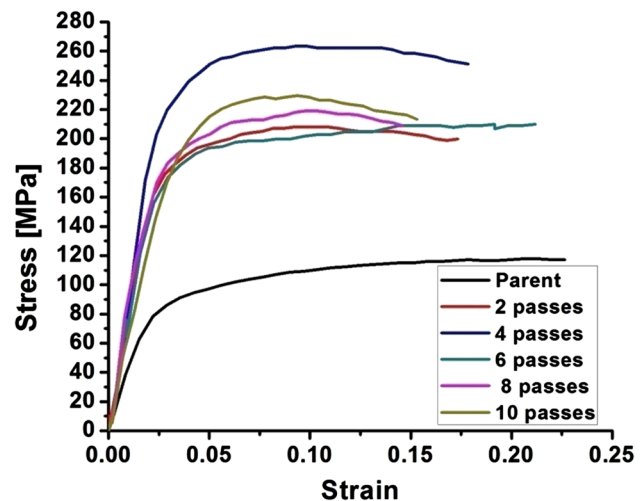

Fig. 14 Stress vs. strain curves for the AA 6063 alloy processed at 130 °C. Data concerning the parent (annealed) as well as CEE-processed AA 6063 alloy after 2, 4, 6, 8 and 10 passes are presented
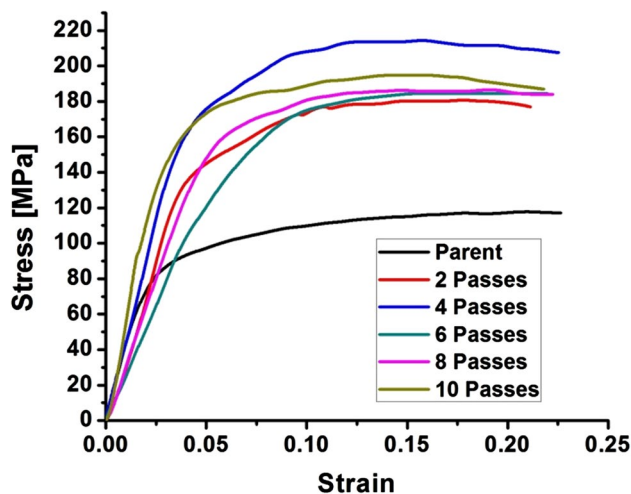

Fig. 13 Stress vs. strain curves for the AA 6063 alloy processed at 200 °C. Data concerning the parent (annealed) as well as CEE-processed AA 6063 alloy after 2, 4, 6, 8 and 10 passes are presented

Figure 15a–c shows the effect of an increase in temperature in the range 260–130 °C on the evolution of hardness in all the three regions (R1–R3). The rate of increase of hardness with strain at 130 °C was the highest, while a homogeneous hardness distribution was obtained at 200 °C and 130 °C (Fig. 15b, c). There was a decrease in hardness with increasing number of passes in the range of 6–10 passes, as the dislocation density and structural evolution got saturated at the higher strains as reported by Valiev and Langdon [8]. In the AA 6063 (4 passes at 200 °C and 130 °C), a significant amount of Mg was in solid solution, leading to solid solution hardening as reported by Babu et al. [14]. At 130 °C, the strain was uniform and grain refinement was maximal (c.f. Figs. 14 and 15c)—Figs. 12, 13 and 15a, b. Consequently, the strength properties were the highest. The imposed strain plays a major role in determining the structural refinement and mechanical properties. Evidently, the mechanical properties were not only affected by the refinement of grains, but also by strain hardening. The precipitates were seen pinning the dislocations and reducing the rate of dynamic recovery. This effect was the highest at the lowest temperature, where the precipitate growth is likely to be the least. This strength increase is in accordance with the Hall–Petch effect. This effect is reduced at 260 °C and 200 °C due to dynamic recovery and dynamic re-crystallization (see Figs. 12 and 14). The specimens processed at 260 °C demonstrated good ductility (22%) after 10 passes and an 18% decrease after 4 passes at 200 °C. The ductility (14%) was the least at 130 °C, as against 23% in the parent (annealed) material.

The microstructure and mechanical properties studies enable the recommendation of 130 °C as the optimal temperature for imparting the required strain without fracture of/cracks in the specimen. A significant rise in hardness after
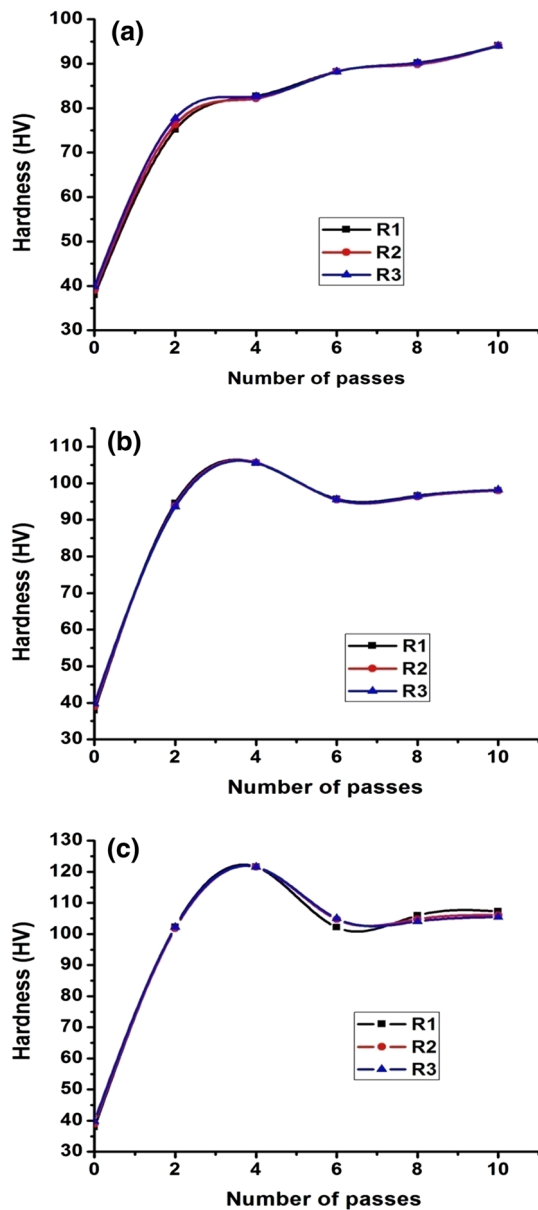
tensile strength—Figs. 13, 14, and 15b, c. The ultimate tensile strength (UTS) was higher after CEE processing by 4 passes at 130 °C due to the dominance of dislocation multiplication over dynamic recovery as reported by Shaeri et al. [27]. The formation of fine grains was the result of a transformation of LAGBs to HAGBs arising as a result of continued deformation. This indicates a lower temperature (130 °C) favoring the conversion of LAGBs into HAGBs with a minimal number of passes, which also accounts for the observed grain refinement. Evidently, all the observations based on the microstructural measurements are consistent with the conclusions drawn based on the measurements of the mechanical properties.

Fig. 15 Hardness of the AA 6063 alloy measured indifferent regions of the specimens processed at **a** 260 °C, **b** 200 °C, and **c** 130 °C: average hardness at R1, R2 and R3 regions vs. number of passes are plotted

4 passes was evident. Plastic deformation at 130 °C allowed shear band formation due to the absence of recovery and re-crystallization. However, this feature did not continue in the range of 6–10 passes, where the curve became flat. In addition, the conversion of LAGBs into HAGBs with strain was facilitated (4 passes at 130 °C). Dynamic recovery and the formation of dislocation bands can be balanced well by processing at 130 °C.

The mechanical properties of a similar alloy processed through twist extrusion (TE) by Zendehdel and Hassani [16] displayed a much smaller improvement in the properties.

This was because in CEE processing, the imposed strain value was as high as ~ 1.7. Therefore, the mechanical properties at 130 °C were higher compared with those obtained in the TE and CEC alloy. The present combination of a semi-die angle (α) of 22.5°, a low temperature and pressing velocity, and the use of a lubricant helped in getting better properties in a smaller number of passes (4 passes). However, a gradual reduction in the rate of increase in strength and a decrease in elongation (8–10%) were observed earlier [16]. However, in this investigation, the reduction in ductility was 14%. Further improvement is possible by optimizing the process variables, viz. the design of the die (semi-die angle), processing temperature, pressing velocity and choice of lubricant.

5 Conclusion

A study on the influence of temperature and degree of strain on AA 6063, subjected to the cyclic expansion extrusion (CEE) process with a semi-die angle (α) of 22.5° at three temperatures of 260 °C, 200 °C, and 130 °C was made. Microstructure evolution was followed using EBSD and TEM analyses. Mechanical properties corresponding to different experimental conditions were measured. The following conclusions were drawn.

1. In the specimen processed at 260 °C, the TEM images reveal the formation of some equiaxed, re-crystallized UFGs of sizes in the range of 500–800 nm and a low fraction of fine grains (1.37%), with a comparatively high fraction of HAGBs (38%). The ultimate tensile strength (UTS) increased by about 56% at the end of 10 passes of CEE. The specimen exhibited an elongation of 22% after 10 passes as against that of the parent material exhibiting a value of 23%.

2. The specimen processed at 200 °C after 4 CEE passes displayed a higher fraction of UFGs (2.82%), with a fairly high fraction of HAGBs (40%). The TEM images reveal the formation of some equiaxed, re-crystallized UFGs of sizes in the range of 200–400 nm. The ultimate tensile strength (UTS) increased strongly by about 83%. The AA 6063 specimen displayed a reduction in elongation after 4 passes and the corresponding figure was 18%.

3. The specimen processed at 130 °C, displayed the formation of equiaxed, re-crystallized nano-grains of sizes in the range of 50-100 nm after 4 passes of CEE. A comparatively higher fraction of HAGBs (45%) and a higher fraction of fine grains (< 1 μm) (7.74%) were seen. Among the three different temperature conditions, processing of the alloy at 130 °C by 4 passes leads to the highest hardness (122 ± 1 HV) due to a near-absence of

recovery. In contrast, at 260 °C, the hardness decreased as a result of grain growth following dynamic recovery and dynamic re-crystallization.

4. The specimen processed at 130 °C, possesses an ultimate tensile strength (UTS) after 4 passes that is higher by about 126% compared with that of the unprocessed material due to the limited significance of recovery. As a base value, the UTS of the parent (annealed) specimen is 118 ± 6 MPa. The AA 6063 specimens after 4 passes at 130 °C displayed an elongation at fracture of 14%, i.e., a notable reduction compared with the 23% elongation of the unprocessed material. However, the ductility loss is significantly less than that seen in the other SPD techniques, which gives rise to the possibility of producing UFG rods of high strength and ductility using the CEE technique.

Compliance with ethical standards

Conflict of interest The authors certify that they do not have any affiliations with any organization, not stated in our address; nor any financial or non-financial interests. The authors report no conflict of interest for the material explained in the manuscript.

Ethical approval Ethical approval and consent to participate are not applicable to this article.

References

1. Sert A, Gürgen S, Çelik QN, Kuşhan MC. Effect of heat treatment on the bending behavior of aluminum alloy tubes. J Mech Sci Technol. 2017;31:5273–8.

2. Babu V, Shanmugavel BP, Padmanabhan KA. On the microstructural homogeneity and mechanical properties of Al 6063 alloy processed by the cyclic expansion extrusion process. J Mater Eng Perform. 2020;29:6870–80. https://doi.org/10.1007/s11665-020-05151-8.

3. Zhu YT, Lowe TC, Langdon TG. Performance and applications of nanostructured materials produced by severe plastic deformation. Scr Mater. 2004;51:825–30.

4. Bay B, Hansen N, Hughes DA, Kuhlmann-Wilsdorf D. Overview no. 96 evolution of fcc deformation structures in polyslip. Acta Metall Mater. 1992;40:205–19.

5. Hughes DA, Hansen N. High angle boundaries formed by grain subdivision mechanisms. Acta Mater. 1997;45:3871–86.

6. Liu Q, Jensen DJ, Hansen N. Effect of grain orientation on deformation structure in cold-rolled polycrystalline aluminium. Acta Mater. 1998;46:5819–38.

7. Panigrahi SK, Jayaganthan R, Pancholi V. Effect of plastic deformation conditions on microstructural characteristics and mechanical properties of Al 6063 alloy. Mater Des. 2009;30:1894–901.

8. Valiev RZ, Langdon TG. Principles of equal-channel angular pressing as a processing tool for grain refinement. Prog Mater Sci. 2006;51:881–981.

9. Mazurina I, Sakai T, Miura H, Sitdikov O, Kaibyshev R. Effect of deformation temperature on microstructure evolution in aluminum alloy 2219 during hot ECAP. Mater Sci Eng A. 2008;486:662–71.

10. Das M, Das G, Ghosh M, Wegner M, Rajnikant V, GhoshChowdhury S, Pal TK. Microstructures and mechanical properties of HPT processed 6063 Al alloy. Mater Sci Eng A. 2012;558:525–32.

11. Rao PN, Singh D, Jayaganthan R. Mechanical properties and microstructural evolution of Al 6061 alloy processed by multi-directional forging at liquid nitrogen temperature. Mater Des. 2014;56:97–104.

12. Lee SH, Saito Y, Sakai T, Utsunomiya H. Microstructures and mechanical properties of 6061 aluminum alloy processed by accumulative roll-bonding. Mater Sci Eng A. 2002;325:228–35.

13. Estrin Y, Vinogradov A. Extreme grain refinement by severe plastic deformation: a wealth of challenging science. Acta Mater. 2013;61:782–817.

14. Babu V, Shanmugavel BP, Padmanabhan KA. On the influence of strain rate and number of passes on grain refinement in Al-Mg-Si alloy processed by cyclic expansion extrusion. J Mater Eng Perform. 2020. https://doi.org/10.1007/s11665-020-05264-0.

15. Lianxi H, Yuping L, Erde W, Yang Y. Ultrafine grained structure and mechanical properties of a LY12 Al alloy prepared by repetitive upsetting-extrusion. Mater Sci Eng A. 2006;422:327–32.

16. Zendehdel H, Hassani A. Influence of twist extrusion process on microstructure and mechanical properties of 6063 aluminum alloy. Mater Des. 2012;37:13–8.

17. Babu V, Shanmugavel BP, Padmanabhan KA. On the influence of temperature and number of passes on the mechanical properties of an Al–Mg alloy processed by cyclic expansion extrusion. Met Mater Int. 2020. https://doi.org/10.1007/s12540-020-00781-y.

18. Sitdikov O, Sakai T, Miura H, Hama C. Temperature effect on fine-grained structure formation in high-strength Al alloy 7475 during hot severe deformation. Mater Sci Eng A. 2009;516:180–8.

19. Thangapandian N, Prabu SB, Padmanabhan KA. Effect of temperature and velocity of pressing on grain refinement in AA5083 aluminum alloy during repetitive corrugation and straightening process. Metall Mater Trans A. 2016;47:6374–83.

20. Pardis N, Talebanpour B, Ebrahimi R, Zomorodian S. Cyclic expansion-extrusion (CEE): a modified counterpart of cyclic extrusion-compression (CEC). Mater Sci Eng A. 2011;528:7537–40.

21. Pardis N, Chen C, Shahbaz M, Ebrahimi R, Toth LS. Development of new routes of severe plastic deformation through cyclic expansion–extrusion process. Mater Sci Eng A. 2014;613:357–64.

22. Babu V, Balasivanandha Prabu S, Padmanabhan KA. Microstructure homogeneity in AA6063 alloy processed by cyclic expansion extrusion. Defect Diffus Forum. 2018;385:223–7.

23. Málek P, Cieslar M, Islamgaliev RK. The influence of ECAP temperature on the stability of Al–Zn–Mg–Cu alloy. J Alloys Comp. 2004;378:237–41.

24. Yamashita A, Yamaguchi D, Horita Z, Langdon TG. Influence of pressing temperature on microstructural development in equal-channel angular pressing. Mater Sci Eng A. 2000;287:100–6.

25. Goloborodko A, Sitdikov O, Kaibyshev R, Miura H, Sakai T. Effect of pressing temperature on fine-grained structure formation in 7475 aluminum alloy during ECAP. Mater Sci Eng A. 2004;381:121–8.

26. Wang YY, Sun PL, Kao PW, Chang CP. Effect of deformation temperature on the microstructure developed in commercial

purity aluminum processed by equal channel angular extrusion. Scr Mater. 2004;50:613–7.

27. Shaeri MH, Shaeri M, Ebrahimi M, Salehi MT, Seyyedein SH. Effect of ECAP temperature on microstructure and mechanical properties of Al–Zn–Mg–Cu alloy. Prog Nat Sci Mater Int. 2016;26:182–91.